Stability Robustness Margin Computation for Structured Real-Parameter Perturbations

Evan Wedell,* C.-H. Chuang,† and Bong Wie‡
University of Texas at Austin, Austin, Texas 78712

An efficient computational method is presented for stability robustness analysis with structured real-parameter perturbations. A generic model of a class of uncertain dynamical systems is used as an example. The parameter uncertainty is characterized by a real scalar perturbation variable. Multilinearity of the closed-loop characteristic polynominal is exploited to permit application of the mapping theorem to calculate the stability robustness margin. It is found that the stability boundary of the perturbation variable exhibits sensitive geometry in the frequency domain, which renders problematic the task of minimizing this variable as a function of frequency. This difficulty is avoided by calculating the minimum distance to the image of the uncertainty domain over frequency as a function of the perturbation. It is also shown that a certain class of uncertain dynamical systems has the required multilinearity property and is thus amenable to the proposed technique.

Nomenclature

K_g = overall loop gain
p = real pole
z = real zero
ζ_p = complex pole damping ratio
ζ_z = complex zero damping ratio
ω_p = complex pole frequency
ω_z = complex zero frequency

I. Introduction

OVER the last 20 years, many advances have been made in the area of robustness analysis and robust control, which may include the mapping theorem,[1] quantitative feedback theory,[2] the singular value concept,[3] H^∞ theory,[4] and Kharitonov's seminal result.[5]

Kharitonov's theorem provides a complete solution to the interval polynomial problem. That is, stability can be determined by examining only four members of the set of all the polynomials obtained by restricting coefficients to the extreme points of their range of variations. This important result is limited by an assumption of independent coefficient perturbations in the characteristic polynomial, which introduces conservative stability bounds if the coefficients are, in fact, functionally dependent.[6] This limitation is partially overcome in Ref. 7, which proves that, if the family of all such polynomials is polytopic in the coefficient space, a necessary and sufficient condition for stability of the entire family is stability of the exposed edges. In Ref. 8, a calculation of the largest spherical perturbation in the parameter space is developed for systems where the polynomial coefficients are linear functions of the uncertain parameters. For the case of multilinear dependence, a domain-splitting algorithm is developed in Ref. 9. The technique is applied with a frequency sweep over the images of the parameter perturbations under the polynomial mapping in a procedure based on the mapping theorem of Ref. 1. This algorithm is extended in Ref. 10 to systems with polynomic dependence of coefficients on parameters. Another version of the domain-splitting algorithm is developed in Ref. 11 to avoid the frequency sweep.

This paper is concerned with the calculation of a stability robustness margin for a feedback control system with uncertain parameters. A computational method is developed, which exploits the mapping theorem of Ref. 1 in a manner similar to Ref. 9 by taking advantage of the multilinearity of the closed-loop characteristic polynomial, and an algorithm is developed to measure the distance from the origin of the convex hull formed by the perturbation image. This is an approximate method that introduces conservative bounds on the uncertainty domain. However, as shown later in this paper, these bounds are nearly exact for a particular uncertain dynamical system considered in this paper. Although the plant parameters are expected to vary in arbitrary combinations, a hypercube in the space of the plant parameters, centered at a nominal point, is assumed as the domain that allows proportional parameter variation. The problem is then to find the stability robustness margin associated with an arbitrary selection of compensator variables. This entails finding the largest hypercube that will fit within the existing, but unknown, region of stability in the plant's parameter space.

One way to perform this calculation is to systematically test points in the parameter space about the nomimal point. At each location, the Routh-Hurwitz stability criteria can be tested or eigenvalues can be explicitly checked. An advantage of this method is that the actual uncertainty bound can be determined without any restrictions on its geometric shape. Unfortunately, excessive computation is required due to the large number of points that must be examined in a multidimensional parameter space.

Alternative procedures are available if the closed-loop characteristic polynomial is multilinear in the uncertain parameters. A polynomial is called multilinear if it can be expressed as an affine relation in any variable while the other variables are held constant. By applying frequency methods in a manner analogous to the Nyquist stability concept, the mapping theorem[1] is used to identify a simple set of bounds at a given frequency. These simple bounds can be used in conjunction with a frequency sweep to ascertain the desired stability margin.[9] The new approach for calculating the stability margin of a nonlinear characteristic polynomial without sweeping in the frequency domain, developed in Ref. 11, has recently been brought to the authors' attention and will be explored in a future work. It is not adopted here.

Received July 10, 1989; presented as Paper 89-3504 at the AIAA Guidance, Navigation, and Control Conference, Boston, MA, August 14-16, 1989; revision received Jan. 15, 1990.

*Graduate Research Assistant, Department of Aerospace Engineering and Engineering Mechanics.

†Postdoctoral Fellow, Department of Aerospace Engineering and Engineering Mechanics.

‡Assistant Professor, Department of Aerospace Engineering and Engineering Mechanics; currently Associate Professor, Department of Mechanical and Aerospace Engineering, Arizona State University, Tempe, AZ. Associate Fellow AIAA.

The paper is organized as follows. A generic example is defined in Sec. II, where the stability robustness problem is formulated. Section III presents an algorithm employing a boundary search in the space of the uncertain parameters. In Sec. IV, the multilinearity property is discussed and the mapping theorem is reviewed. Section V develops a procedure to determine the minimum distance from the origin to the nearest outer edge of the convex hull formed by the perturbation image at a fixed frequency. A frequency search method is presented in Sec. VI. This approach is rendered problematic by the appearance of sensitive geometry for the example of this paper. Section VII introduces a new frequency search approach that avoids this problem. In Sec. VIII, a comparative sensitivity locus study is performed. Section IX discusses the main results of the paper.

II. Problem Formulation

Consider a single-input, single-output control system, as shown in Fig. 1. The plant, shown in Fig. 2, is an undamped two-mass-spring model that is a generic representation of uncertain dynamical systems, such as flexible space structures.[12] The control input and sensor output are associated with different bodies, which represents the noncollocated structural control problem. It is assumed that the mass and spring stiffness parameters are uncertain with nominal values set to unity. The system is described by the transfer function

$$\frac{y(s)}{u(s)} = P(s) = \frac{(k/m_1m_2)}{s^2\{s^2 + k[(1/m_1) + (1/m_2)]\}} \tag{1}$$

as indicated in Fig. 2. The compensator is assumed to have the following generic form:

$$C(s) = \frac{K_g[(s/z)+1]\ [(s^2/\omega_z^2) + (2\zeta_z s/\omega_z) + 1]}{[(s/p)+1)][(s^2/\omega_p^2) + (2\zeta_p s/\omega_p) + 1]} \tag{2}$$

The uncertainty is defined by a cubic perturbation parameterized in terms of a scalar perturbation variable ϵ as follows:

$$\begin{aligned} 1-\epsilon \le\ & k/k_o \le 1+\epsilon \\ 1-\epsilon \le\ & m_1/m_{1_o} \le 1+\epsilon \\ 1-\epsilon \le\ & m_2/m_{2_o} \le 1+\epsilon \end{aligned} \tag{3}$$

where $k_o = m_{1_o} = m_{2_o} = 1$ are nominal values. If values are assigned to the compensation variables K_g, z, p, ω_z, ω_p, ζ_z, and ζ_p, the stability robustness margin ϵ_s is defined as the largest ϵ corresponding to a cube within which all points yield stable

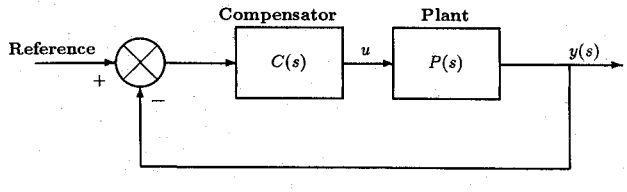

Fig. 1 Single-input, single-output closed-loop system.

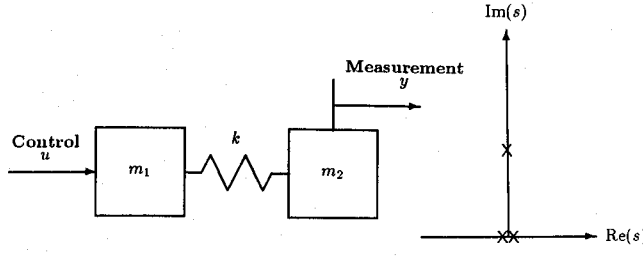

Fig. 2 Generic model of an uncertain dynamical system.

closed-loop systems. The problem is to compute ϵ_s given a set of K_g, z, p, ω_z, ω_p, ζ_z, and ζ_p. A nonminimum phase compensator,[12] with $K_g = 0.015$, $z = 0.15$, $p = 10.0$, $\zeta_z = -0.5$, $\zeta_p = 0.5$, and $\omega_z = \omega_p = 1.4142$, is used here as an example.

The closed-loop characteristic polynomial of the system can be found as

$$\begin{aligned} \Delta(k, m_1, m_2, s) &= \sum_{i=0}^{7} a_i(k, m_1, m_2) s^{7-i} \\ &= a_0 s^7 + a_1 s^6 + \cdots + a_6 s + a_7 \end{aligned} \tag{4}$$

where

$$\begin{aligned} a_0 &= \left(\frac{1}{p\omega_p^2}\right) m_1 m_2 \\ a_1 &= \left(\frac{1}{\omega_p^2} + \frac{2\zeta_p}{p\omega_p}\right) m_1 m_2 \\ a_2 &= \left(\frac{1}{p} + \frac{2\zeta_p}{\omega_p}\right) m_1 m_2 + \left(\frac{1}{p\omega_p^2}\right)(m_1 + m_2)k \\ a_3 &= m_1 m_2 + \left(\frac{1}{\omega_p^2} + \frac{2\zeta_p}{p\omega_p}\right)(m_1 + m_2)k \\ a_4 &= \left(\frac{1}{p} + \frac{2\zeta_p}{\omega_p}\right)(m_1 + m_2)k + K_g\left(\frac{1}{z\omega_z^2}\right)k \\ a_5 &= (m_1 + m_2)k + K_g\left(\frac{1}{\omega_z^2} + \frac{2\zeta_z}{z\omega_z}\right)k \\ a_6 &= K_g\left(\frac{1}{z} + \frac{2\zeta_z}{\omega_z}\right)k \\ a_7 &= K_g k \end{aligned}$$

The coefficients a_i are symmetric with respect to the masses m_1 and m_2. Since $m_{1_o} = m_{2_o}$, it is only necessary to examine half of the cubic perturbation to determine stability, that is, above or below the plane with $m_1 = m_2$, as shown in Fig. 3. This symmetric property is exploited to save computational time.

III. Boundary Search in Parameter Space

A direct approach to computing ϵ involves a systematic testing of parameter values in the neighborhood of the nominal point. At each location, stability can be determined by checking the Routh-Hurwitz criteria or finding the zeros of the characteristic polynomial $\Delta(k, m_1, m_2, s)$ in s. The search entails selection of a grid with mesh size $\delta\epsilon$. The stability boundary is then bracketed by increasing ϵ in increments of $\delta\epsilon$ and testing grid points on the surface of the corresponding cubes. Once an unstable point is detected, $\delta\epsilon$ is gradually reduced and grid point testing proceeds to refine the cube size ϵ until an acceptable accurate value of ϵ_s is obtained. An algorithm to perform this task follows.

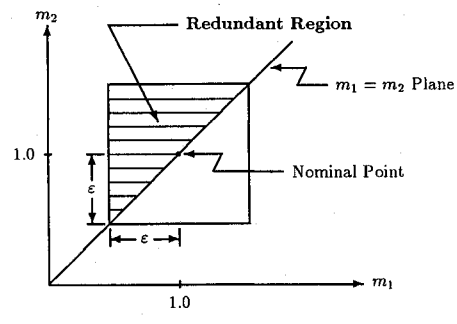

Fig. 3 Redundancy in perturbation due to m_1 and m_2 symmetry in $\Delta(k, m_1, m_2, s)$, k out of page.

1) Test nominal point for stability ($\epsilon = 0$). If not stable, STOP. Set $\delta\epsilon$.
2) Replace ϵ with $\epsilon + \delta\epsilon$.
3) Test points on surface of cube of size ϵ with mesh $\delta\epsilon$.
4) If an unstable point is found, go to step 5. Otherwise, go to step 2 and repeat.
5) Replace ϵ with $\epsilon - \delta\epsilon$.
6) Replace $\delta\epsilon$ with $\delta\epsilon/2$.
7) Test points on surface of cube of size ϵ with mesh $\delta\epsilon$.
8) If an unstable point is found, replace ϵ with $\epsilon - 2\delta\epsilon$ and go to step 7. Otherwise go to step 9.
9) Replace ϵ with $\epsilon + \delta\epsilon$.
10) Test points on surface of cube of size ϵ with mesh $\delta\epsilon$.
11) If an unstable point is found, go to step 5.
12) If $\delta\epsilon \leq \sigma$, STOP. Otherwise, go to step 6.

The quantity σ is a small positive number used as a convergence criterion. In step 7, it is not necessary to test all grid points because this cube is tested previously in the algorithm at twice the mesh size. In other words, if the grid points p on a given face of the cube are indexed by integers i and j as

$$p = (1 \pm \epsilon)e_1 + (1 + i\delta\epsilon)e_2 + (1 + j\delta\epsilon)e_3 \tag{5}$$

where e_1, e_2, e_3 are unit vectors in the directions of k, m_1, and m_2. It is not necessary to test points for which i and j are both even since these points have already been tested.

The main drawback of this procedure is the computational burden of testing a large number of points as $\delta\epsilon$ becomes small or ϵ becomes large. The number of points N that must be tested on the surface of a hypercube of dimension n and size ϵ is given by

$$N = 2^{n-3}(n^2 - n)(2\epsilon/\delta\epsilon - 1)^2 + n2^{n-1}(2\epsilon/\delta\epsilon - 1) + 2^n \tag{6}$$

where $2^{n-3}(n^2 - n)$ is the number of faces, $n2^{n-1}$ the number of edges, and 2^n the number of corner points. For $n = 3$, this reduces to

$$N = 6(2\epsilon/\delta\epsilon - 1)^2 + 12(2\epsilon/\delta\epsilon - 1) + 8 \tag{7}$$

Since $\Delta(k, m_1, m_2)$ is symmetric in m_1 and m_2, the number of points that need to be tested becomes

$$N = 3(2\epsilon/\delta\epsilon - 1)^2 + 8(2\epsilon/\delta\epsilon - 1) + 6 \tag{8}$$

If $\epsilon = 0.5$ and $\delta\epsilon = 2^{-10} \approx 9.77 \times 10^{-4}$, then $N = 3{,}147{,}777$ points must be examined for a value of ϵ accurate to three decimal places. Many cubes are tested in the iterative process, which further compounds the computation. As can be seen from Eq. (6), the amount of computation increases dramatically with dimension.

This algorithm has been implemented in a computer program that determines stability of a point by means of the Routh-Hurwitz criteria. This program is written in Fortran 77 and requires over 1700 s on a CDC CYBER 170/750 to compute the margin $\epsilon_s = 0.338$ for the example of this paper to an accuracy of $\delta\epsilon = 2^{-12} \approx 1.22 \times 10^{-4}$. This approach is considerably slower than the frequency search method developed later in this paper.

IV. Multilinearity and the Mapping Theorem

A polynomial $\delta(m,s)$ is said to be multilinear in $m = [m_1,\ldots,m_n]^T$ if for any of the m_i it is possible to write $\Delta(m,s)$ as $\Delta(m,s) = am_i + b$ where a and b are functions of $m_1, m_2,\ldots, m_{i-1}, m_{i+1},\ldots,m_n$, and s. As can be seen in Eq. (4), the closed-loop characteristic polynomial for the example of this paper is multilinear in k, m_1, and m_2. This multilinearity property also holds for higher-order structural models. To see this, consider a system of n masses connected by $n - 1$ springs, as shown in Fig. 4. The equations of motion for this system are given by

$$M\ddot{q} + Kq = u \tag{9}$$

where

$$q = [q_1,\ldots,q_n]^T$$

$$u = [u_1,\ldots,u_n]^T$$

$$M = \text{diag}(m_1,\ldots,m_n)$$

$$K = \begin{bmatrix} k_1 & -k_1 & 0 & \cdots & 0 \\ -k_1 & k_1 + k_2 & -k_2 & & 0 \\ 0 & -k_2 & \ddots & & \vdots \\ \vdots & & & k_{n-2} + k_{n-1} & -k_{n-1} \\ 0 & & \cdots & -k_{n-1} & k_{n-1} \end{bmatrix}$$

The transfer functions for each channel are then given by

$$P_{ij} \triangleq \frac{q_i}{u_j} = \frac{N_{ij}}{\det[Ms^2 + K]} \tag{10}$$

where $i = 1,\ldots,n$, $j = 1,\ldots,n$, and N_{ij} is a cofactor of $Ms^2 + K$.

For a mechanical system described by Eqs. (9) and (10), the following theorem holds:

Theorem 1. 1) $\det[Ms^2 + K]$ is a multilinear function of the m_i and the k_i. 2) N_{ij} are each multilinear functions of the m_i and the k_i. 3) The closed-loop characteristic polynomial for $P_{ij}(s)$ with controller $u_j = -C(s)q_i$ is a multilinear function of the m_i and k_i.

The first part of the theorem can be seen by noticing that square terms in k_i generated by the main diagonal terms in $\det[Ms^2 + K]$ are cancelled by products of the symmetric off-diagonal elements. This result can be proved by induction on n. The second assertion can be shown to follow from the first by arranging the minors of $[Ms^2 + K]$ in terms of principal minors. If any of these transfer functions are placed in a feedback loop with compensator $C(s) = N_C(s)/D_C(s)$, the resulting closed-loop characteristic polynomial can be expressed as

$$\Delta(\cdot, s) = N_P(\cdot, s)N_C(s) + D_P(\cdot, s)D_C(s) \tag{11}$$

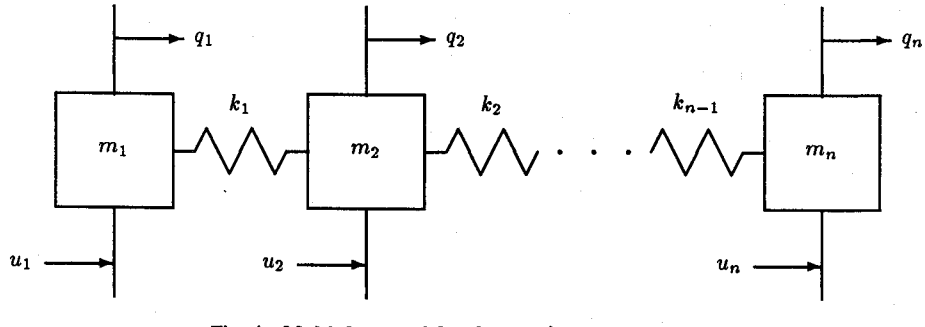

Fig. 4 Multi-degree-of-freedom spring-mass system.

where $P(s) = N_P(s)/D_P(s)$. Since the numerator and denominator polynomials N_C and D_C of the compensator do not depend on the parameters k_i and m_i, multilinearity of N_P and D_P implies multilinearity of Δ. Multilinearity of the closed-loop characteristic polynomial is required for application of the frequency search approach of this paper. Hence, the previous important result indicated the potential for generalization of the method to higher-order mechanical systems with uncertain mass and stiffness matrices.

In the frequency-response approach, stability is tested by investigation of the $j\omega$-axis behavior of $\Delta(k, m_1, m_2, s)$. For a given frequency ω, the function $\Delta(\cdot, j\omega)$ maps an ϵ perturbation of k, m_1, and m_2 into a closed region of the complex plane. If Δ is multilinear in k, m_1, and m_2, a useful characterization of this region can be obtained through the mapping theorem of Ref. 1.

Theorem 2 (Mapping Theorem). For any ω, the image of an n-dimensional rectangular region within the parameter space under the mapping $\Delta(\cdot, j\omega)$ is contained in the convex hull formed from the images of the n-dimensional rectangle's vertices.

Convex hull designates the locus of points p obtained from a finite set of points $p_1, p_2, \ldots, p_l$ in the space $\Re^n$ as follows:

$$p = \sum_{i=1}^{l} \lambda_i p_i, \qquad \lambda_i \geq 0 \text{ and } \sum_{i=1}^{l} \lambda_i = 1 \tag{12}$$

Consider the example illustrated in Fig. 5. A cube in the space of the parameters is shown with vertices **1,2,...,8**. These vertices are mapped to the points **1′,2′,..., 8′** on the Δ plane for a given ω. The solid lines connecting these points on the Δ plane correspond to the cube's edges. The convex hull is the four-sided polygon **1′,2′,7′,8′**. The shaded area is the Δ-plane image of the cube, which lies within the convex hull. In general, this polygon constitutes a conservative boundary for the Δ-plane image since the actual bound between some of the exterior corner points may describe a concave parabolic curve rather than a straight line, as illustrated in Fig. 5.

For the system considered in this paper, these curved boundaries are absent. The polygon boundary is either exact, or for some frequencies, the true boundary follows a straight line that lies inside the polygon and corresponds to a mapped edge of the cube. Two sample plots are shown in Figs. 6. In this case, the convex hull of mapped corner points is a good approximation to the actual boundary. Note that there are only six distinct mapped corner points due to m_1, m_2 symmetry.

The absence of curved boundaries is a consequence of another interesting property of the Δ-plane image. For fixed k, perturbation in m_1 and m_2 maps to a line.

Theorem 3. The image of a plane parallel to the m_1 and m_2 axes for arbitrary fixed k under the mapping $\Delta(k, m_1, m_2, j\omega)$ defined by Eq. (4) with constant ω is a line on the complex plane. Any two such lines comprising the images of two planes corresponding to two distinct values of k are parallel.

To see this, express the real and imaginary parts of $\Delta(\cdot, j\omega)$ as follows:

$$x = \mathrm{Re}(\Delta) = -a_1\omega^6 + a_3\omega^4 - a_5\omega^2 + a_7 \tag{13a}$$

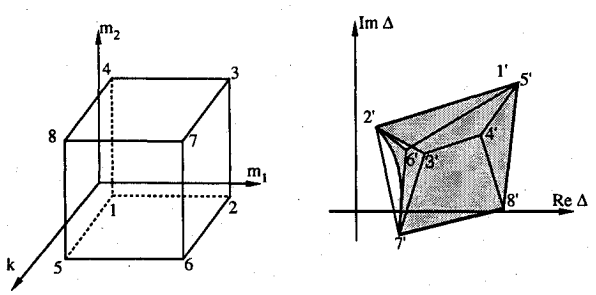

Fig. 5 Parameter-space cube and its Δ-plane image for a fixed ω.

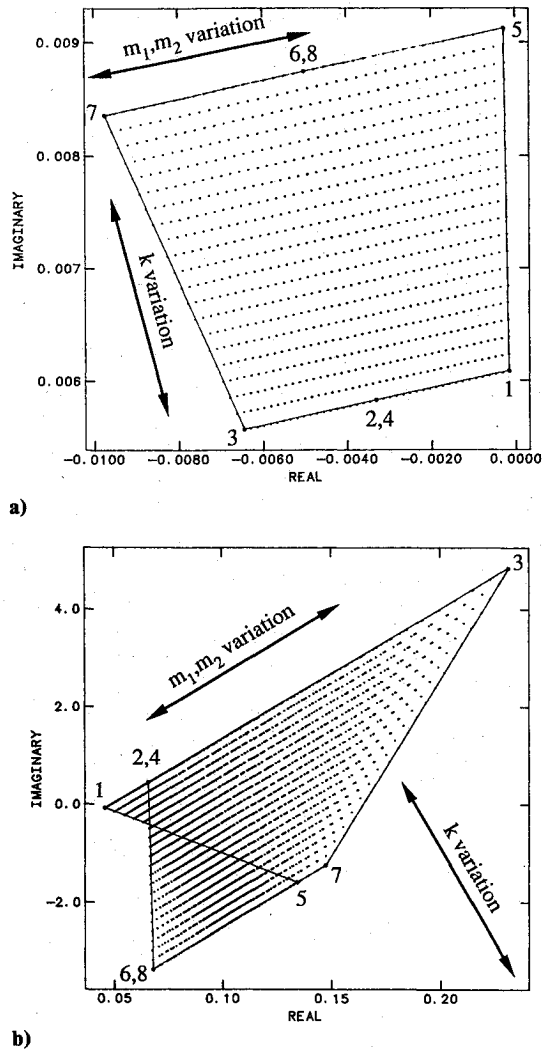

Fig. 6 Sample plots of Δ-plane images of a cubic perturbation for fixed ω: a) $\epsilon = 0.2$, $\omega = 0.1$; b) $\epsilon = 0.6$, $\omega = 1.3$.

$$y = \mathrm{Im}(\Delta) = -a_0\omega^7 + a_2\omega^5 - a_4\omega^3 + a_6\omega \tag{13b}$$

Substituting in the expressions for the a_i from Eq. (4) and rearranging terms yields the vector relation

$$p = bm_1m_2 + c(m_1 + m_2) + d \tag{14}$$

where $p = [x,y]^T$, and b,c,d are constant vectors with components:

$$b_1 = \omega^4 - \left(\frac{1}{\omega_p^2} + \frac{2\zeta_p}{p\omega_p}\right)\omega^6$$

$$b_2 = \left(\frac{1}{p} + \frac{2\zeta_p}{\omega_p}\right)\omega^5 - \left(\frac{1}{p\omega_p^2}\right)\omega^7$$

$$c_1 = \left(\frac{1}{\omega_p^2} + \frac{2\zeta_p}{p\omega_p}\right)k\omega^4 - k\omega^2$$

$$c_2 = \left(\frac{1}{p\omega_p^2}k\right)\omega^5 - \left(\frac{1}{p} + \frac{2\zeta_p}{\omega_p}\right)k\omega^3$$

$$d_1 = K_g k - K_g\left(\frac{1}{\omega_z^2} + \frac{2\zeta_z}{z\omega_z}\right)k\omega^2$$

$$d_2 = K_g\left(\frac{1}{z} + \frac{2\zeta_z}{\omega_z}\right)k\omega - K_g\left(\frac{1}{z\omega_z^2}\right)k\omega^3$$

Examination of these coefficients reveals that the $c = -kb/\omega^2$, and hence,

$$p = \mu b + d \tag{15}$$

where $\mu = m_1 m_2 - k(m_1 + m_2)/\omega^2$. Since Eq. (15) is linear in the lumped parameter μ, the locus of points p comprising the image of points (k, m_1, m_2) for fixed k must be a line. Furthermore, p is independent of k, so that any two lines corresponding to distinct values of this parameter must be parallel. This result can be observed in Figs. 6.

The straight line character of the Δ-plane image's boundary can be shown by first noting that the one-parameter family of planes perpendicular to the k axis lying in the cube maps to a family of parallel line segments. An endpoint of any such line segment must lie on the image of an edge parallel to the k axis, and multilinearity of Δ guarantees that any edge of the cube maps to a straight line. A detailed proof is omitted.

V. Minimum Distance to the Convex Hull

In applying the mapping theorem to stability robustness analysis, it is useful to establish a measure of the minimum distance d from an edge of a polygon to the origin, and then to determine the ϵ at which $d = 0$. To this end, d is defined as the minimum (Euclidean) length from the origin to the perimeter of the polygon, as shown in Figs. 7. In order to develop an algorithm to calculate d, some preliminary problems must be addressed.

A first step is to find d for a line segment, as indicated in Fig. 8. An analytical expression can be obtained through consideration of the constrained optimization problem given below:

$$\min d^2(p_3) = x_3^2 + y_3^2 \tag{16}$$

subject to

$$p_3 = \lambda p_2 + (1-\lambda)p_1, \qquad 0 \le \lambda \le 1 \tag{17}$$

with p_1, p_2 given.

The solution to this problem is as follows. First, calculate

$$\lambda = -\frac{x_1(x_2-x_1) + y_1(y_2-y_1)}{(x_2-x_1)^2 + (y_2-y_1)^2} \tag{18}$$

If $\lambda \ge 1$, then $p_3 = p_2$, and

$$d = \sqrt{x_2^2 + y_2^2} \tag{19}$$

If $\lambda \le 0$, then $p_3 = p_1$, and

$$d = \sqrt{x_1^2 + y_1^2} \tag{20}$$

Otherwise $0 < \lambda < 1$, and

$$d = \frac{|x_1 y_2 - x_2 y_1|}{\sqrt{(x_2-x_1)^2 + (y_2-y_1)^2}} \tag{21}$$

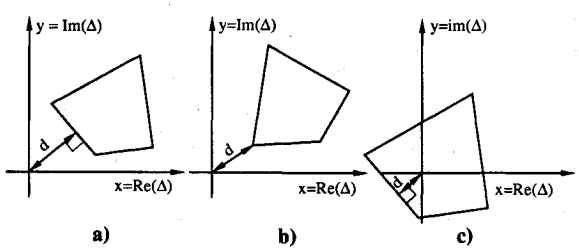

Fig. 7 Minimum distance from the origin to a polygon.

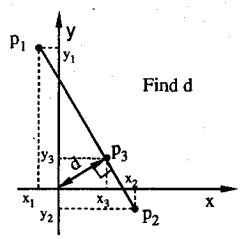

Fig. 8 Minimum distance to a line segment.

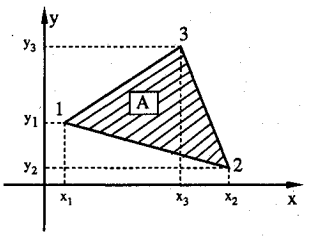

Fig. 9 Triangle with ordered vertices.

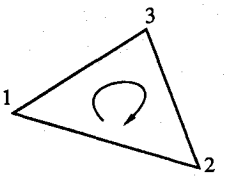

Fig. 10a Negative ordering.

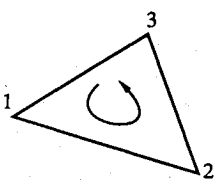

Fig. 10b Positive ordering.

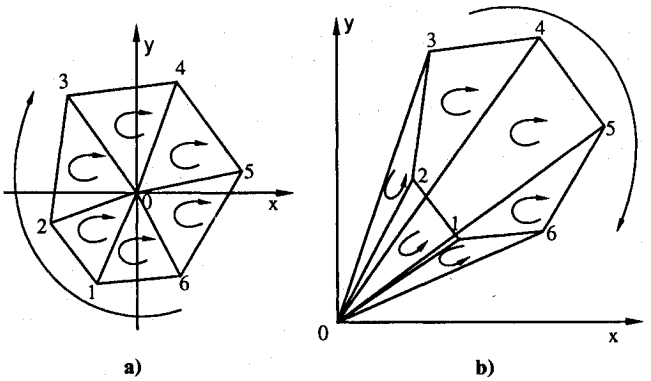

Fig. 11 Operation to determine zero encirclement: a) interior case; b) exterior case.

Next, a technique is required to determine whether the origin is encircled by the polygon (as in Fig. 7c). This is done by first noting that the area of a triangle can be computed by the formula[13]

$$A = \frac{1}{2}\begin{vmatrix} x_1 & y_1 & 1 \\ x_2 & y_2 & 1 \\ x_3 & y_3 & 1 \end{vmatrix} \tag{22}$$

where x_i and y_i are the coordinates of the triangle's vertices, as indicated in Fig. 9. This quantity is negative or positive depending on whether the vertices are ordered clockwise or counterclockwise (Figs. 10a and 10b). Location of a vertex, the third one, say, at the origin yields the relation

$$\begin{vmatrix} x_1 & y_1 & 1 \\ x_2 & y_2 & 1 \\ 0 & 0 & 1 \end{vmatrix} = x_1 y_2 - x_2 y_1 \tag{23}$$

This relation is applied to determine encirclement of the origin by partitioning the polygon into triangles joined at the origin, ordering the vertices in a consistent manner, and calculating the area of each triangle. For example, in Figs. 11, clockwise ordering is employed in the computation of $A(0,1,2)$, $A(0,2,3)$,$A(0,3,4)$, ..., $A(0,6,1)$ where

$$A(0,i,j) = \tfrac{1}{2}(x_i y_j - x_j y_i) \tag{24}$$

If the origin lies in the interior of the polygon, as depicted in Fig. 9a, then all the areas will be negative

$$A(0,1,2),A(0,2,3), \ldots, A(0,6,1)<0 \tag{25}$$

However, if the origin is outside the polygon, then some of the areas will be positive. For example, in Fig. 11b, we have

$$A(0,1,2),A(0,2,3),A(0,6,1)>0 \tag{26a}$$

$$A(0,3,4),A(0,4,5),A(0,5,6)<0 \tag{26b}$$

In summary, let **1,2,...,*n*** denote consecutive vertices of a convex planar polygon in a clockwise direction. Let **0** denote the origin. If at least one of $A(0,1,2)$, $A(0,2,3)$, ..., $A(0,n-1,n)$, $A(0,n,1)$, where $A(0,i,j)$ is defined by Eq. (24), is positive, then the origin is not encircled by the polygon. Note that the ½ may be omitted in actual computation of A since it is the sign of A that is of importance here.

Another issue concerns the identification of boundary points. Given a collection of points p_i, $i = 1, \ldots, m$ in a plane, which of these lie on the convex hull, that is, which comprise the vertices of the (convex) polygon that bounds the collection? The problem is illustrated in Fig. 12a, in which the dashed lines demark the boundary to be identified. The algorithm used to perform this task is given below:

1) Input $x_1,y_1, \ldots, x_m,y_m$.
2) Find n such that

$$y_n = \min_j(y_j), j = 1, \ldots, m$$

3) Exchange the settings of L_1 and L_n.
4) Find n such that

$$\phi_{L_n} = \max_j(\phi_{L_j}), j = 2, \ldots, m$$

5) Exchange the settings of L_2 and L_n.
6) Set i to 2.
7) Find n such that

$$\alpha_{L_i L_n} = \max_j(\alpha_{L_i L_j}), j = i+1, i+2, \ldots, m, 1$$

8) If $n = 1$, then output L, i and STOP.
9) Exchange the settings of L_j and L_n.
10) Replace i with $i + 1$ and go to step 7.

The algorithm makes use of an index array L, which is initially configured in ascending order. The angles ϕ_{L_j} and $\alpha_{L_i L_j}$ are defined in Figs. 12b and 12c, respectively. The procedure is to find the lowest point of the collection and then to locate successive boundary points in a clockwise direction. As an example, consider the set of points $p_1, \ldots, p_8$ in Fig. 12a. In this case, the initial setting of the index array is

$$L = (1,2,3,4,5,6,7,8)$$

In steps 2 and 3, the algorithm finds the point p_4 with the lowest value of y and exchanges the corresponding index L_4 with that in the first position L_1, to yield

$$L = (\underline{4},2,3,1,5,6,7,8)$$

Steps 4 and 5 calculate the orientation of ϕ_{L_j} of all the other points about p_4. The point p_7 with the largest such angle is identified as the next boundary point and its index L_7 is exchanged with L_2 so that

$$L = (4,\underline{7},3,1,5,6,2,8)$$

A third boundary point p_5 is determined in step 7 as the point with the largest angle α_{7,L_j} about p_7 measured counterclockwise from the line segment joining p_7 and p_4. The indices L_5 and L_3 are exchanged in step 9 to get

$$L = (4,7,\underline{5},1,3,6,2,8)$$

Steps 7–10 are repeated to identify the remaining boundary points, resulting with the following indexing:

$$L = (4,7,5,\underline{8},3,6,2,1)$$

$$L = (4,7,5,8,\underline{3},6,2,1)$$

Hence, the convex hull is the polygon **4, 7, 5, 8, 3**. Note that in each iteration of step 7, calculation of $\alpha_{L_i L_j}$ is avoided for previously identified boundary points, except $p_{L_1} = p_4$, the testing of which is required to terminate the loop.

The previous methods to compute the shortest distance to a line segment, determine encirclement of the origin, and identify boundary points can be combined to find the shortest distance d to the convex hull of points $p_1, \ldots, p_m$ as follows:

1) Input $x_1, y_1, \ldots, x_m,y_m$.
2) Find n such that

$$y_n = \min_j(y_j), j = 1, \ldots, m$$

3) Exchange the settings of L_i and L_n.
4) Find n such that

$$\phi_{L_n} = \max_j(\phi_{L_j}), j = 2, \ldots, m$$

5) Calculate $D(L_1, L_n)$ and store the result in d.
6) Calculate $A(0,L_1,L_n)$ and store the sign of the result in z.
7) Exchange the settings of L_2 and L_n.
8) Set i to 2.
9) Find n such that

$$\alpha_{L_i L_n} = \max_j(\alpha_{L_i L_j}), j = i+1, i+2, \ldots, m, 1$$

10) Calculate $D(L_{i-1}, L_n)$ and store the result in d^*.

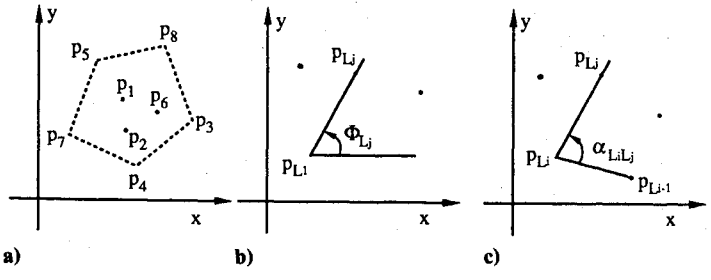

Fig. 12 Determination of boundary points: a) example problem; b) geometry defining ϕ_{Lj}; c) geometry defining $\alpha_{L_i L_j}$.

11) If d^* then replace d with d^*

12) If $z<0$ then calculate $A(0,L_{i-1},L_n)$ and replace z with sign of the result.

13) If $n=1$ then replace d with the product $z \cdot d$, output d and STOP.

14) Exchange the settings of L_j and L_n.

15) Replace i with $i+1$ and go to step 9.

The function $A(0,i,j)$ is defined by Eq. (24) and $D(i,j)$ designates computation of the distance from the origin to the line segment joining $p_i=[x_i,y_i]^T$ and $p_j=[x_j,y_j]^T$ by means of Eqs. (18–21). The output d is the minimum distance d^* to each line segment of the convex hull. The sign of d indicates encirclement of the origin deduced from the computation of $A(0, i,j)$ for the boundary points with clockwise ordering, as depicted in Fig. 11. If $d<0$, the origin lies inside the convex hull.

In implementing this algorithm on the computer, some computational issues need to be addressed. First, if two boundary points p_i and p_j are close together so that $\Delta x=x_i-x_j$ and $\Delta y=y_i-y_j$ are smaller than the machine precision, Eq. (21) should not be used to compute d^*. Instead, use Eqs. (19) or (20) depending on which yields a smaller d^*. Another problem occurs if two points p_j and p_k are far from p_i so that the angles ϕ_j and ϕ_k or α_{ij} and α_{ik} are indistinguishable. In this case, compute the determinant:

$$A=\begin{vmatrix} x_j & y_j & 1 \\ x_k & y_k & 1 \\ x_i & y_i & 1 \end{vmatrix} \tag{27}$$

If $A>0$, choose p_k in steps 4 or 9 of the algorithm, otherwise choose p_j.

VI. Frequency Search Method

According to the mapping theorem, the system is stable in a cubic perturbation ϵ if, overall ω, the mapping of the cube on the Δ plane by the characteristic polynomial $\Delta(\cdot, j\omega)$ does not include the origin. An increase in ϵ effects an expansion of this Δ-plane region, which intersects the origin at $\epsilon=\epsilon_s$, the stability robustness margin. For the case in which ω is fixed, the image of a parameterized cube is a family of polygons. An ϵ satisfying $d(\epsilon,\omega)=0$ yields a polygon intersecting the origin for the given choice of ω. The smallest such ϵ overall ω is ϵ_s.

This suggests a method of finding ϵ_s by minimizing ϵ over ω subject to $d(\epsilon,\omega)=0$. At each ω, the ϵ satisfying the constraint is found by means of a suitable numerical technique, bisection in this case. Examination of a polar plot of the nominal characteristic polynomial $\Delta(k_o, m_{1_0}, m_{2_0}, j\omega)$ indicates a reasonable range for the search to be $0\le\omega\le\omega_{max}=10$, where $\Delta(\cdot, j\omega)\neq 0$ for $\omega_{max}<\omega<\infty$.

Unfortunately, this procedure is hindered by numerical difficulties arising from a sensitive geometry of the $d(\epsilon,\omega)\le 0$ region on the ϵ,ω plane. A computer program employing this method is unable to detect $d(\epsilon,\omega)=0$ except at $\epsilon=1$, even for the smallest stepsize $\delta\omega=0.001$ rad/s. At this value of ϵ, the cubic perturbation includes the point $k=m_1=m_2=0$. This point lies outside the region of physically allowable k, m_1, m_2, and it is unstable since the coefficients a_i of $\Delta(k, m_1, m_2, s)$ vanish in Eq. (4). Hence, $\epsilon=1$ is an upper bound of possible stability margin values. However, by the grid search in parameter space (cf. Sec. III), the margin is previously determined to be $\epsilon_s=0.338$.

To explain the discrepancy, it is possible to numerically detect $d(\epsilon,\omega)\le\sigma$, where σ is a small positive number, and, thus, find admissible regions within which may lie the locus of points such that $d(\epsilon,\omega)\le 0$. A plot reveals a distinct reduction in ϵ about certain critical frequency bands. As $\sigma\to 0$, the widths of these regions shrink with respect to ω and become almost impossible to detect for $\sigma\le 1.0\times 10^{-20}$. Figure 13 shows sample $d(\epsilon,\omega)$ contours, which approach spike-like shapes as σ is reduced. It appears that the $d(\epsilon,\omega)\le 0$ points form very narrow bands and possibly one-dimensional curves along the floor of these σ valleys.

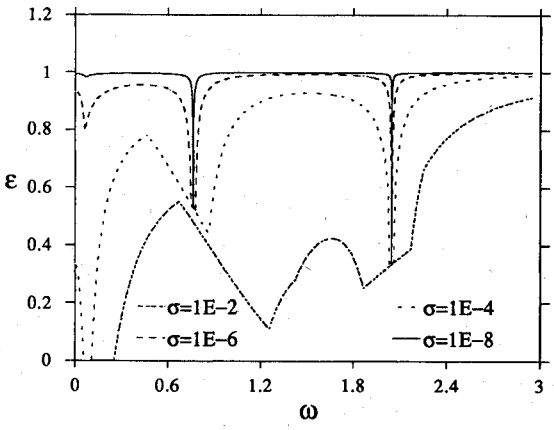

Fig. 13 $d(\epsilon,\omega)=\sigma$ contours.

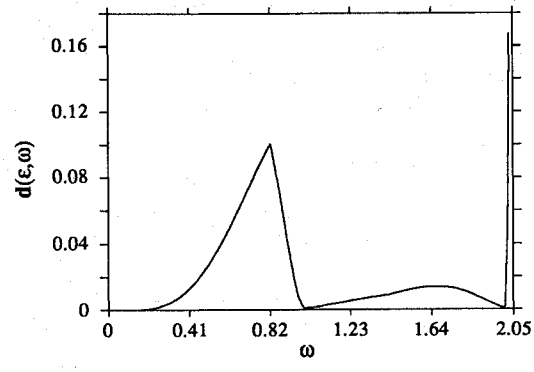

Fig. 14 Sample plot of $d(\epsilon,\omega)$ for $\epsilon=0.32$.

This particular characteristic of the example in this paper will cause the approaches of Refs. 9 and 10 to fail. It is difficult to find the critical ω at which the $d(\epsilon,\omega)\le 0$ bands may be situated by use of conventional search techniques. It may be possible to use a recursive approach in which σ is systematically reduced. Valleys are located while σ is relatively large (on the order of 10^{-2}, say) and an estimate of the $d(\epsilon,\omega)\le 0$ region is refined as $\sigma\to 0$ until some adequate criterion is met. This procedure has not been implemented. Instead, another approach is considered in which the order of the search in ϵ and ω is reversed.

VII. Alternative Frequency Search Method

In this approach, the margin ϵ_s is determined by finding the largest ϵ for which the minimum of $d(\epsilon,\omega)$ over ω is positive. This is equivalent to the previous method, but the d vs ω curves do not exhibit the sensitive behavior encountered earlier. See Fig. 14 for a sample plot of d vs ω. At each ϵ, a one-dimensional search is performed to find minimum values of $d(\epsilon,\omega)$. The golden ratio method is used to achieve convergence for each minimum. Bisection is then used to find $\epsilon=\epsilon_s$ at which the minimum $d(\epsilon,\omega)$ is zero. At each ϵ, more than one minimum is present, and so the search algorithm is invoked repeatedly to find all the extrema to determine which is the global minimum. A Fortran program employing this method calculates a value of $\epsilon=0.338$ to nine-place accuracy on the CDC CYBER in less than 20 s.

VIII. Discussion

The frequency search methods are considerably faster than grid testing due to the reduction of an n-dimensional bound-

ary search to a two-dimensional parameter optimization problem. The reduction in the dimension of the parameter variations simultaneously adds complexity to the problem in the form of several local minimums, hence, the need for successive searches to make sure all the minimums are found and compared. Locating the $d(\epsilon,\omega) \leq 0$ region turns out to be problematic in numerical application. Minimizing ϵ over ω by determining $d(\epsilon,\omega) = 0$ at each ω is not possible for the example of this paper because of the near singular geometry of the $d(\epsilon,\omega) \leq 0$ region on the ϵ,ω plane. That is, the minimum ϵ appear in spikes that are not possible to locate by simple point sampling methods.

Another approach is suggested by reversing the order in which the two parameters are searched. In this case, d is minimized over ω for each ϵ. The algorithm then seeks the largest ϵ at which minimum d is positive. This approach is equivalent to that mentioned earlier. However, the d vs ω curves do not exhibit the sensitive geometry of the $\epsilon \ni d(\epsilon,\omega) = 0$ vs ω curves. The minimum d can thus be found using conventional methods. This approach has been implemented and appears to work well. It is recommended that more numerical examples be investigated to further understand the difficulty encountered with the prior method.

The frequency search method is applicable to any plant with a transfer function that is multilinear with respect to the uncertain parameters in the numerator and denominator polynomials. A certain class of dynamical systems, including flexible space structures, has the multilinearity property. In this paper, an analytical expression for the closed-loop characteristic function is employed. This is by no means required in practice as the characteristic polynomial can be calculated from expressions for the loop transfer function numerator and denominator by Eq. (11).

IX. Conclusions

A computationally efficient method has been presented for the stability robustness analysis with structured real-parameter uncertainty. Multilinearity of the closed-loop characteristic polynomial was exploited to apply the mapping theorem. It was also shown that a certain class of uncertain dynamical systems such as flexible space structures possesses the multilinearity property and is thus amenable to the proposed technique.

Acknowledgments

This research was supported in part by NASA Langley Research Center (CSI GI program NAG-1965) and Goddard Space Flight Center. The authors would like to thank Frank Bauer at NASA GSFC for his sponsoring this research for possible implementation to INCA program.

References

[1]Zadeh, L. A., and Desoer, C. A., *Linear System Theory,* McGraw-Hill, New York, 1963.

[2]Horowitz, I., *Synthesis of Feedback Systems,* Academic, New York, 1963.

[3]Doyle, J. C., and Stein, G., "Multivariable Feedback Design: Concepts for a Classical and Modern Synthesis," *IEEE Transactions on Automatic Control,* Vol. AC-33, No. 2, 1981, pp. 4–16.

[4]Zames, G., and Francis, B., "Feedback Minimax Sensitivity and Optimal Robustness," *IEEE Transactions on Automatic Control,* Vol. AC-26, No. 5, 1983, pp. 585–600.

[5]Kharitonov, V. L., "Asymptotic Stability of an Equilibrium Position of a Family of Systems of Linear Differential Equations," *Differential'nye Uraveniya,* Vol. 14, No. 11, 1978, pp. 1483–1485.

[6]Barmish, B. R., "New Tools for Robustness Analysis," *Proceedings of the IEEE Conference on Decision and Control*, Austin, Dec. 1988.

[7]Bartlett, A. C., Hollot, C. V., and Lin, H., "Root Locations of an Entire Polytope of Polynomials: It Suffices to Check the Edges," *Mathematics of Control, Signals and Systems,* Vol. 1, 1987, pp. 61–71.

[8]Biernacki, R. M., Hwang, H., and Bhattacharyya, S. P., "Robust Stability with Structured Real Parameter Perturbations," *IEEE Transactions on Automatic Control,* Vol. AC-32, No. 6, 1987, pp. 495–506.

[9]De Gaston, R. R. E., and Safonov, M. G., "Exact Calculation of the Multiloop Stability Margin," *IEEE Transactions on Automatic Control,* Vol. AC-33, No. 2, 1988, pp. 187–190.

[10]Sideris, A., and de Gaston, R. R. E., "Multivariable Stability Margin Calculation with Uncertain Correlated Parameters," *Proceedings of the IEEE Conference on Decision and Control*, Athens, 1986.

[11]Sideris, A., and Pena, R. S., "Fast Computation of the Multivariable Stability Margin for Real Interrelated Uncertain Parameters," *Proceedings of the American Control Conference,* Atlanta, 1988.

[12]Wie, B., and Byun, K.-W., "New Generalized Structural Filtering Concept for Active Vibration Control Synthesis," *Journal of Guidance, Control, and Dynamics,* Vol. 12, No. 2, 1989, pp. 147–154.

[13]Klein, F., *Elementary Mathematics from an Advanced Standpoint: Geometry,* Dover, New York, 1939, pp. 3–10.